HPM generation in atmospheric air

Mladen M. Kekez

High-Energy Frequency Tesla Inc., (HEFTI), 1200 Montreal Road, NRC-Site, Building M-51, Ottawa, Canada, K1A 0R6, E-mail: mkekez@hefti.ca, Web-site: www.hefti.ca

Abstract

A new method of High Power Microwave (HPM) generation in atmospheric air is proposed. It embraces the idea developed in the design of CO_2, N_2 and the excimer lasers. The Marx generator pumps the energy into (the runaway electrons of) the corona (glow) discharge that is situated in the cavity. The cavity containing 100% reflector/mirror and partially transparent reflector/mirror, is arranged in such a way that RF/microwave can bounce back and forth through the gain (corona (glow)) medium. This electromagnetic (radiation) wave causes the space charge waves in the glow plasma. This process enables the bunching of high-speed electrons in the retarding zones of the space charge waves and the transfer of the energy from the corona (glow) discharge into the radiation wave. The best single frequency results are obtained when the resonant cavity is tuned at a frequency of 730-765 MHz, 1.21 GHz, 1.69 GHz or 1.96 GHz. The output microwave radiation is emitted through the partially transparent reflector/mirror.

With 6-stage Marx generator charged at 25 kV per stage, the plasma interacting with the microwave wave may yield a sudden (>100 times) increase in the HPM power in the resonator. When this occurs, the maximum electrical field recorded inside the resonant cavity exceeds 580 kV/cm at a frequency of 1.69 GHz. Full understanding of the corona plasma response to the electromagnetic wave responsible for the build up of HPM energy inside the resonator is required. The current study is related to the use of the Magneto-Cumulative Generator (MCG) as the HPM source.

1. Introduction

It is generally understood that the HPM sources stand for the source of coherent radiation that are produced through the interaction of an intense relativistic electron beam propagating in the vacuum with an electromagnetic structure [1].

The idea of HPM generation in atmospheric air is a great departure from the existing knowledge on classical microwave production. If the idea is to be understood, it may be necessary to present all the experimental steps taken in the formulation of the new concept.

Most references that could be cited here belong to the design of CO_2, N_2 and excimer lasers. For example, Sarjeant *et al* [2] describes the production of volume glow discharge in a scalable multi-atmosphere rare gas halide laser capable of producing the output energy of 0.6 J at wavelength of 248.3 nm from an active volume of 0.18 liter.

Interest in the proposed new method of HPM generation has been stimulated not only by its low cost and simplicity of the design in comparison to the relativistic electron beam devises, but also by the possibility of being perhaps suitable for the MCG application.

2. Helical antenna under pulsed power conditions

Let us consider the case when the helical (end fire) antenna designed according to Kraus *et al* [3] is subject to the impulse from the Marx generator. The schematic of the set-up is given in Figure 1.

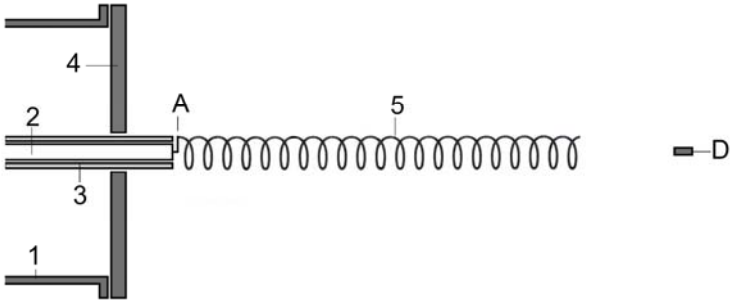

Figure 1. Schematic 1 is the metallic enclosure of the 6-stage Marx generator, 2 the hot electrode of the generator, 3 the plexiglass tube, 4 the metallic flange, 5 the helix and D is the detector.

For the antenna, the flange, 4 is the ground reflector/plane. In the experiment, the flange is of 40 cm diameter. Copper tubing, of 6 m long, of 0.635 cm diameter is used to form the helix of 6.35cm inner diameter, D. According to Kraus *et al*, the wavelength of antenna, λ is equal to the circumference, and the pitch between the turns is made to be $\lambda/4$.

To avoid unnecessarily stressing of the charging resistive network of the Marx generator during the discharge cycle, it is wise to connect a resistor (say R_A of 300 Ω) at the output. This resistor is connected at the point A on one side and the other side is attached to the metallic enclosure.

Many precautions were taken to avoid the partial corona discharges at the “triple point”: where the solid (plexiglass tube) dielectric, 3 meets the metallic flange, 4 and gaseous dielectric as well as the point where the resistor, R_A is connected.

The experimental results are shown in Figure 2 and the PSpice simulation of these experimental data are presented in Figure 3. Figure 4 indicates that the RF/HPM radiation from this set-up is sufficiently powerful to ignite the neon bulbs.

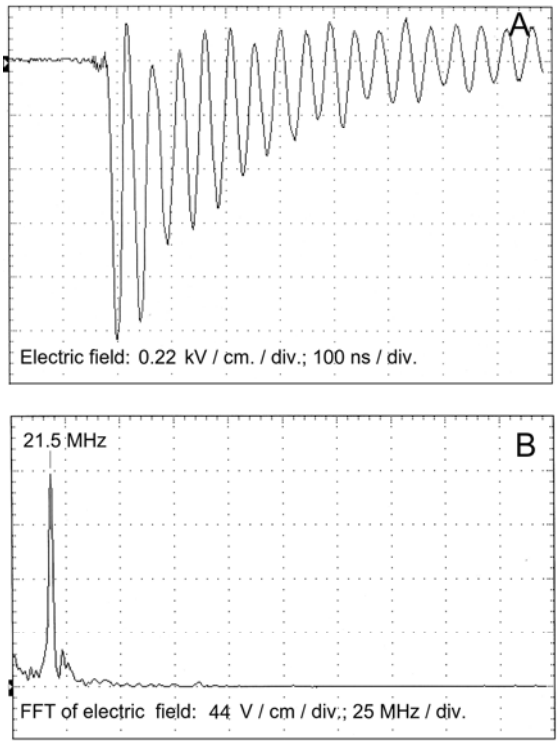

Figure 2. Frame A shows the electric field, E recorded with the electric field probe at the distance of 1.12 m. Frame B is FFT of the field. These data are obtained with 6-stage Marx generator used

6-stage Marx generator is charged to 25 kV/stage and the total energy stored in the Marx generator is 84 J.

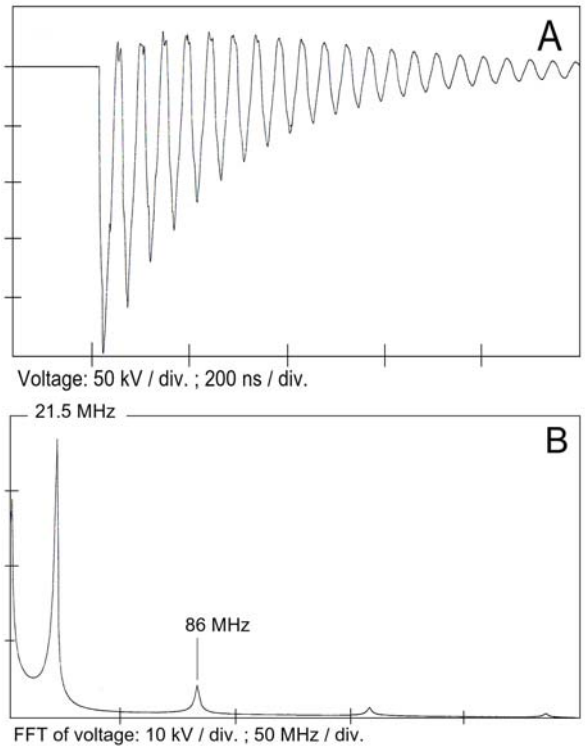

Figure 3. Frame A is PSpice computer simulation of the open-circuit line of characteristic impedance of 130 Ω to get the voltage waveform at the end of the helix. **Frame B** is FFT of frame A.

6-stage Marx generator is approximated by a 7.5 nF capacitor charged to V = 150 kV. The internal impedance of the generator, R_G is assumed to be 5 Ω.

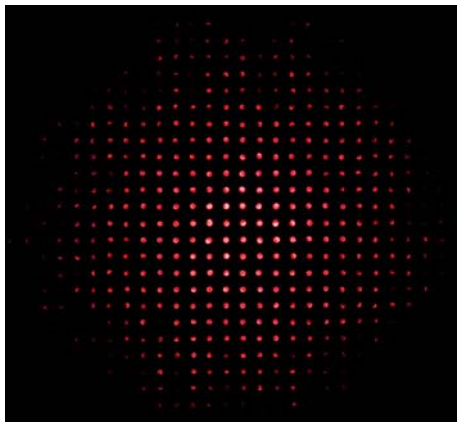

Figure 4. Ignition of neon bulbs by RF/HPM radiation that is produced by a 10-stage Mini-Marx generator. The generator is charged to 25 kV/stage and stores 6.25 J. The bulbs are placed on plywood across the radiation's beam to get the radiation's pattern. The separation between the bulbs is 2.54 cm. The board is placed at a short distance away from the helix. 6-stage Marx generator containing the energy of 84 J provides the same ignition pattern as 10-stage Mini-Marx generator.

2.1 PSpice simulation

The experimental results of Fig. 2 can be tentatively understood by using the PSpice program. The essential feature is that the helical line is an open-circuit line, characterized by the characteristic impedance, Z_o and the transit time delay, T_o. The frequency of 21.5 MHz shown in Fig. 2, Frame B corresponds to $4T_o$. From the geometry of the helical line in respect to the flange, 4, Z_o is estimated to be 130 Ω.

6-stage Marx generator is approximated by a 7.5 nF capacitor charged to V= 150 kV. The internal impedance of the generator, R_G is taken to be 5 Ω. The maximum energy, E that the helical line receives, is

$$E= [(2V)^2 / Z_o] 2T_o= [(300\ kV)^2 / 130\ \Omega] 2 *11.62\ ns=16\ J. \quad (1)$$

If R_G is small and Z_o large, this energy will bounce back and forth in the helical line: between the open circuit at the exit of the line and the input of the line.

The main uncertainty in the simulation is the value of the impedance at the triple point. The computer runs show that the impedance at this point does not correspond to the value of the parallel combination of Z_o and the resistor, R_A. The PSpice program does not provide the method to account for the loss of energy by radiation from the helix. Also, there is the possibility that some partial discharges are taking place and they are decreasing the impedance. To get Fig. 3, the impedance of 20 Ω is taken in the computation at the triple point

The experimental data of Fig. 2 shows the pulses are of triangular shape. This implies that high frequency components are “lost”. To remove these high frequencies in the simulations, 50-pF capacitor is attached at the end of the helical line. The reason for the loss of these frequencies will be discussed in the following section.

2.2 Coherence effects

The detailed study of first radiation pulse is performed in the anechoic chamber to understand the coherence effects. Because the anechoic chamber is of limited size, the Mini-Marx generator is used instead of 6-stage Marx generator. The same helical line is employed.

The first radiation pulse recorded close to the helical antenna is shown in Fig. 5, Frame C. The first part of the pulse has fast (<1ns) rise-time. The rise-time of the initial portion of the pulse is of similar shape as the output voltage pulse when the generator is terminated with the matching resistive load.

The second portion of the pulse has a long (15 ns) rise-time. This is due to the fact that, the helical line is an open-circuit enabling the voltage to double its value at the output.

The electric field measurements show that, the electric field is of equal strength within the radius of 10.5±1 cm (and within the area of 346 cm^2) where the center of this radius can be placed in the centre of Fig. 4. At the distance of 12 cm, the electric field, E measured is 20 kV/cm. See Fig. 6, Frame A. The power density is $E^2/(120\pi)$ = (20 $kV/cm)^2/(120\pi)$= 1.06 MW/cm^2.

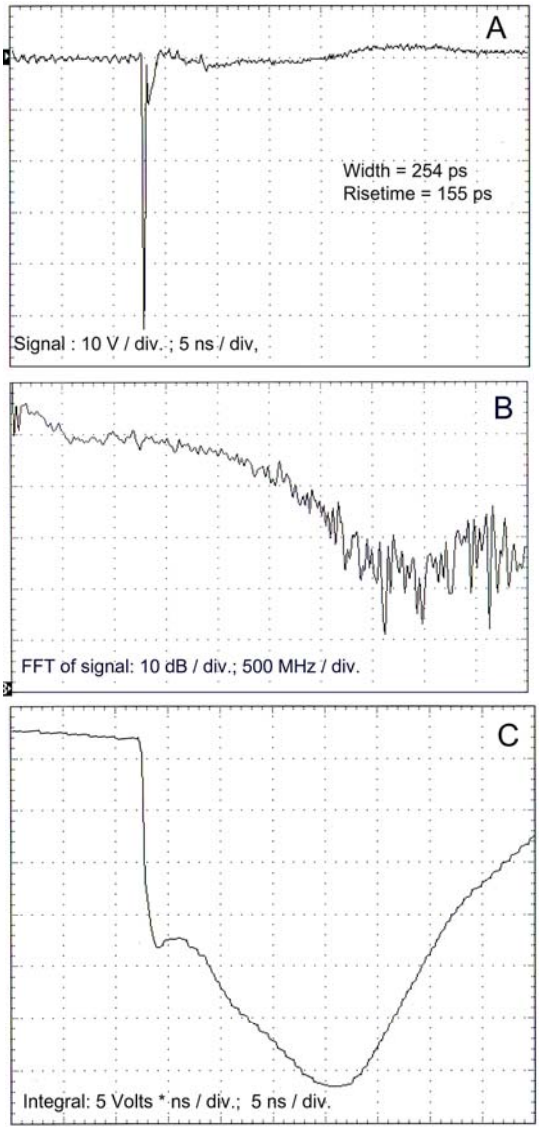

Figure 5; Data at 17 cm. Frame A is the B-dot signal. Frame B is the FFT of A. Frame C is the integral of the B-dot signal to get the magnetic field. B-dot probe is calibrated in the TEM-cell. to get the electric field (to correspond to the integral of B-dot)

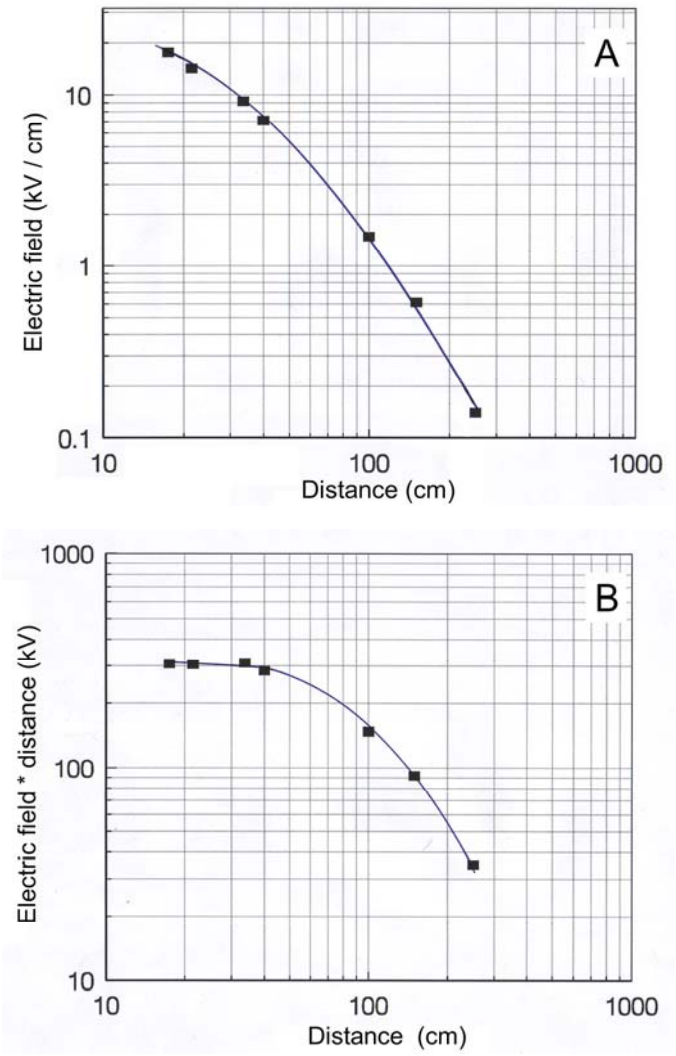

Figure 6; Frame A is the plot of the electric field, E in kV/ cm *vs* distance in cm. Frame B is the graph of the product of the electric field and distance *vs* distance. Here, E is recorded by E field probe.

These numbers suggest that the generation of RF/HPM power of radiation at the exit of the helical antenna can approach 1GW range if a small 10-stage Mini-Marx generator is charged to the voltage higher than 25 kV per stage.

To understand the limitation of this statement, the measurements are made as a function of the distance in the longitudinal direction

It was observed that the shape of radiation waveform became distorted as the distance is increased. At larger (>30 cm) distance, FFT starts to have many "valleys" in comparison to the smooth FFT shown in Fig. 5, Frame B.

At larger distances the radiation waves at various frequencies start interacting / interfering with one another at some distance. They can add constructively or subtract destructively causing the destructive subtractions of high (>100 MHz) frequency bands. Hence, the electric field falls much faster than 1/r, where r is the distance. See Fig. 6, Frame A.

At the time, $t=\tau=0$ at the exit of the helical antenna, the degree of coherence can be considered perfect, whereas it drops significantly at the time τ_c. The time τ_c is defined by the propagation distance, L from a coherent source to a point where an electromagnetic wave maintains a specified degree of coherence. The wave is travelling the distance. L in time, τ_c with the speed of light.

From the Heisenberg uncertainty principle, it is shown [4] that the coherence effects are not be pronounced for the temporal duration of the pulse, $\Delta t = L/c$, (where *c* is the speed of light) if:

$$\Delta t \, \Delta f \, . \, 1 \qquad (2)$$

Here, Δf is the spectral bandwidth of the source.

Eq. 2 sets the criteria for the design of the ultra-wide band system and offers the explanation why it is necessary to have a coherent radiation source if the HPM radiation pulse is to propagate over a large distance.

An example of the ultra-wide band system is put forward by Baum *et al* [5]. To get a fairly flat spectral content over one to two decades (tens of MHz to several GHz), Baum *et al* have achieved the width of the pulse, Δt to be as short as 100 ps. They have also succeeded in making the product (r*E) of the electric field, E times the distance, r to be constant (.5.3 MV) well over the distance of 200 m. Because Δt is small in Baum *et al* set-up, the unwanted consequence is that, the energy content of any ultra-wide system is rather limited.

From Fig. 6, Frame B we see that the product: (r*E) is constant (=300kV) and that the distance, of 40 cm corresponds to the propagation distance, L used in getting Eq. 2. In

comparison to the work by Baum *et al* [5], the reflector behind the helical line is not used to get Fig.6.

3. Experimental set-up with the corona (glow) plasma

The goal of the experimental set-up shown in Fig. 7 is to get a coherent radiation at the single frequency. The set-up combines the geometry shown in Fig. 1 with the arrangement that are used to produce the gas discharge lasers: i.e., CO_2, N_2 and KrF* lasers.

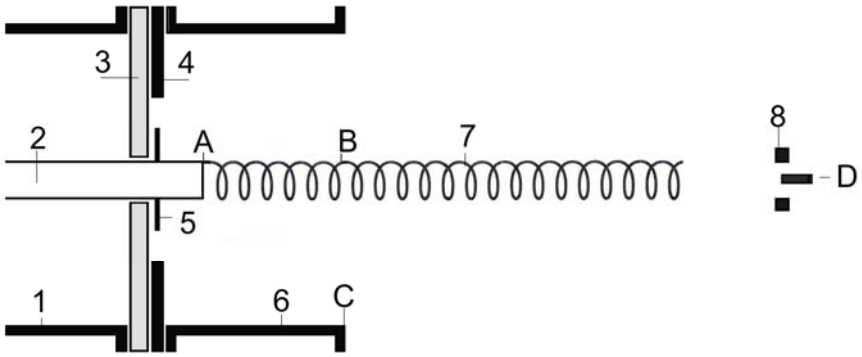

Figure 7; Schematic of the experimental set-up. 1 is the metallic enclosure of the 6-stage Marx generator, 2 the hot electrode of the generator, 3 the plexiglass flange, 4 the metallic flange, 5 set of electrodes, 6 the section of the metallic cylinder/tube, 7 the helix, 8 HPM reflector and D is the detector.

The flange, 4 is the high reflector (a 100% reflector mirror in laser terminology). 8 is the partially transparent reflector (like the output lens in the lasers). The corona (glow) discharges occur inside the metallic cylinder, 6 between the helix, 7 and the cylinder, 6. To get the rapid energy deposition into a glow discharge, the UV pre-ionization is provided by the array of 9 spark sources formed between the needle electrodes, 5 and the flange, 4. These spark sources are placed in the same plane but 20^o apart. The corona (glow) plasma is considered here to be the "gain (plasma) medium". The cavity is formed between the metallic flange, 4 and the partially transparent reflector, 8 to facilitate resonance. The output microwave radiation beam is emitted through the partially transparent reflector, 8. Behind the detector, D and the partially transparent reflector, 8, the absorbing blocks are placed to minimize the reflections of the radiation from the walls of the laboratory.

The metallic cylinder, 6 performs several functions. By introducing the cylinder, the impedance of the helical line, Z_o is decreased. According to Eq. 1, this means a better energy transfer from the Marx generator into the helical line. If the cylinder of smaller diameter is used, Z_o will fall further and the energy transfer will be enhanced.

The cylinder, 6 can also be viewed as the waveguide in which TE_{11} mode has the smallest cut-off frequency, f_c. For the circular waveguide of 15.24 cm inner diameter D_i, f_c is 576 MHz. For D_i of 11.43 cm, f_c is 1.538 GHz.

It may be useful to state the meaning of the term: resonance.

4. Resonance

The frequency of the radiation is determined by the condition of the resonance. If the corona plasma is absent in the cavity, the round trip distance, *2d*, is equal to an integral number of wavelengths λ of the wave:

$$2d = N\lambda \text{ where } N = \{1, 2, 3... \} \quad (2)$$

This can also be expressed in terms of frequency:

$$f = N\lambda / 2d \quad (3)$$

In the experiments, the frequency of the resonator, *f* of Eq. 3 is set to match certain strong frequency line, f_g (caused by the runaway electrons) of the corona (glow) discharge when the resonator is absent. Afterwards, the cavity is tuned to compensate for the presence of plasma in the cavity.

Kekez [6] has observed that the spark/glow discharges have a wide frequency spectrum with many strong frequency lines that are reaching up to 16 GHz (equals to the bandwidth of the oscilloscope used). However, when the same spark/glow discharges are put in the resonant cavity, the radiation at the single frequency is obtained.

5. Experimental results

In Fig. 7, the cylinder is of 15.24 cm diameter and its length is approximately 1/4 of the length of the helical line. By introducing the cylinder, the impedance, Z_o is abruptly changed at the end of the cylinder. This sudden change in Z_o means discontinuity. Because of this, there are reflections of the voltage impulse from this discontinuity towards the flange 4 and back again. This effect is similar in nature as the one shown in Fig. 2. Hence, in addition to the frequency of 21.5 MHz indicated in Fig. 2, Frame B, the frequencies of about 80 MHz are also present,

By setting N of Eq. 2 to be 16, the system is tuned to radiate at 1.21 GHz. The experimental data are shown in Figs. 8 and 9. When Fig. 8 is compared to Fig. 2, the explanation for the separate burst of the pulses shown in Fig. 8 is obvious: each pulse containing only 1.21 GHz frequency component in Fig.8 corresponds to the single (broad band frequency) pulse provided by the Marx generator to the corona plasma discharge.

By increasing the charging voltage of the generator, Fig. 9 is obtained. The frequency spectrum shown in Fig. 10 is the same as the one shown in Fig. 8, Frames B and C. The main difference is that we have a single pulse radiating at frequency of 1.21 GHz instead of the burst of pulses radiating at frequency of 1.21 GHz as shown in Fig. 8.

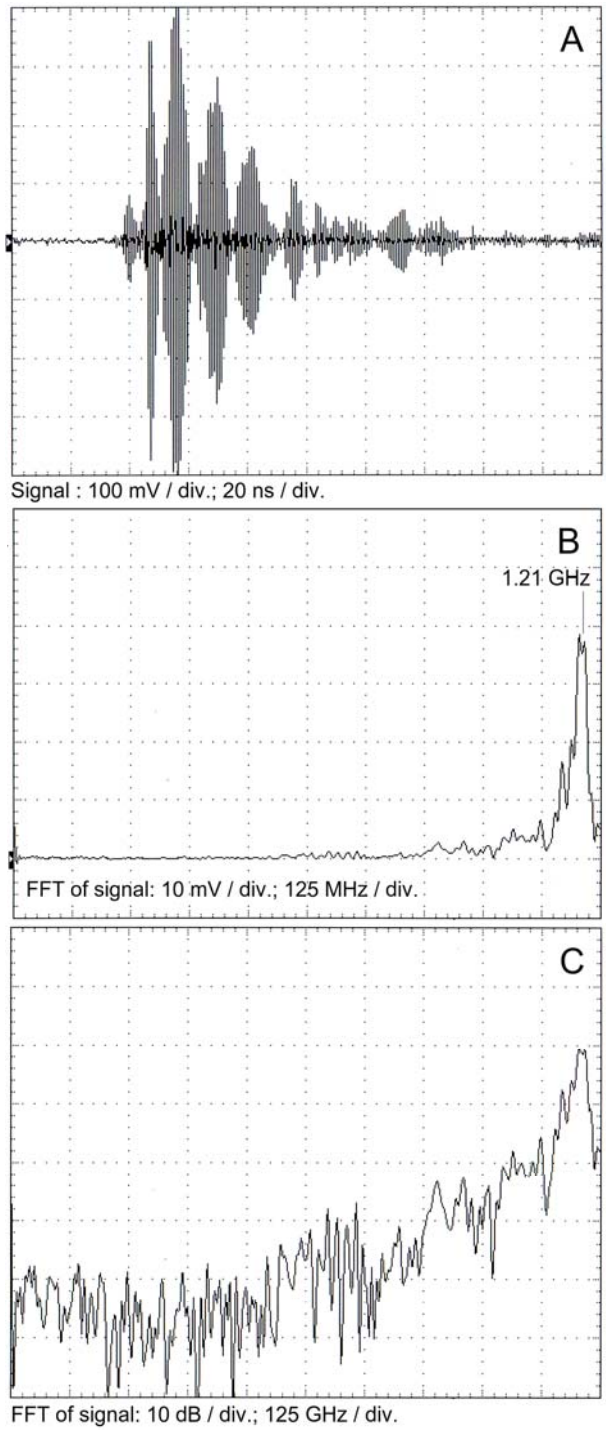

Figure 8. Experimental data**; Frame A** is the signal recorded at the time scale of 10 ns/div. **Frames B** and **C** are the FFT of the signal, shown on the linear and logarithmic scale. B-dot probe is used. 6-stage Marx is charged to 23 kV/stage.

To demonstrate that the phenomenon under consideration is valid for different experimental set-up, Fig. 11 is presented. Here, the cylinder, 6 of Fig, 7 has D_i of 11.43 cm. Instead of helix, 7 a solid brass electrode of 5 cm diameter and 6 cm height is used. The partially transparent reflector, 8 is placed at the distance where *N* of Eq. 2 is 2.

To better understand the experimental data: Figures 8 to 11, the current measurements are attempted for the set-up shown in Figure 7.

The MCG-like experiments show that Rogowski coil also behaves as a receiving helical antenna, i.e., Rogowski coil measures, the combined signals due to the current and the radiations. Therefore, Rogowski coil is an unsuitable tool to measure the current.

The shunt was applied in the study and it was attached between the points B and C that are indicated in Figure 7. To bridge the gap, a short lead was used. This lead represents the inductor; hence the bandwidth of the shunt is limited.

To make the measurement possible, it was necessary to arrange the system to resonate at low frequency, i.e., 730 MHz. Figure 12 shows the data before the shunt is introduced. Figures 13 to 16 are the records when the shunt is present.

By comparing the frames A and B in Fig. 13 we have clear evidence that plasma is present inside the volume of the cylinder, 6. We see that when the HPM radiation shown in Figure 13, Frame A would fall, the current through the shunt, shown in Figure 13, Frame B will rise.

To increase the level of the current of the corona discharge, narrow aluminum strips were placed over certain portion of the helix that is placed inside the cylinder. The idea is to introduce the sharp edges at the helix hence to facilitate larger amount of the coronas.

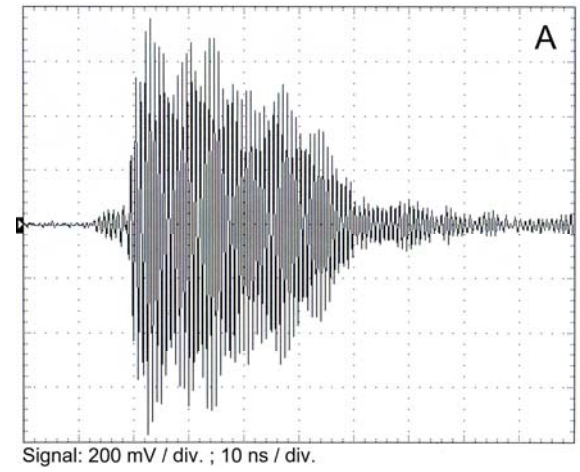

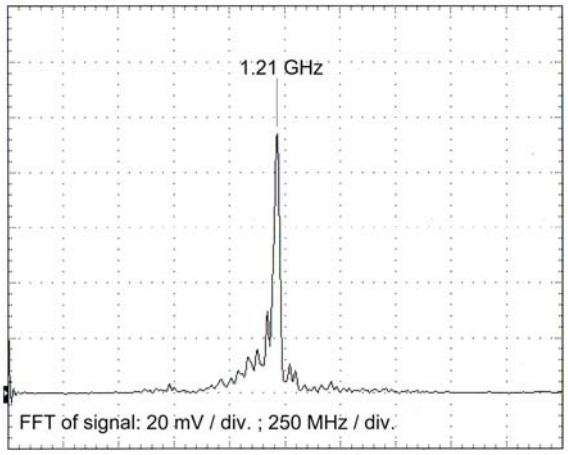

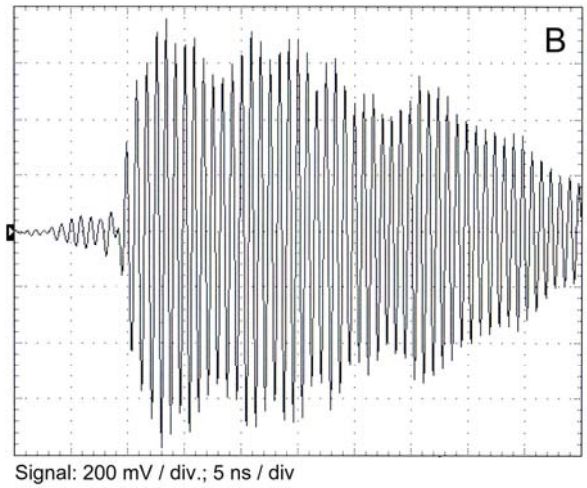

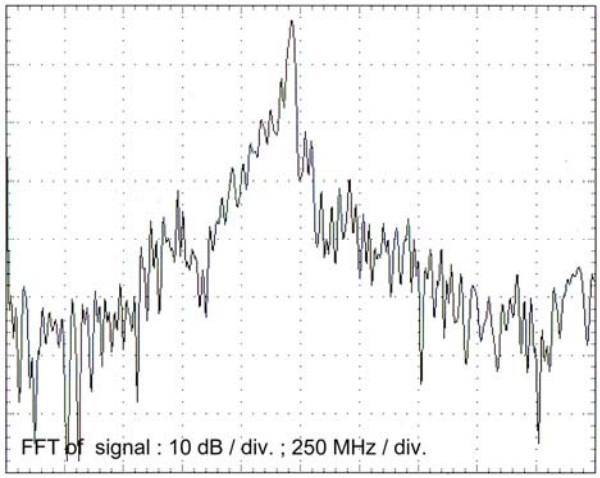

Figure 9; Frame A: Signal recorded at the time scale of 10 ns per division. Frame B is the same signal presented on the time scale of 5 ns per division. 6-stage Marx generator is charged to 25 kV per stage and the energy stored in the generator is 84 J. B-dot probe is used to record the signal.

Figure 10; FFT of the signal shown in Fig. 9, frame A. B-dot probe is calibrated in the TEM-cell. For frequency of 1.21 GHz, the amplitude of the signal of 1 Volt corresponds to the electric field of 2.63 kV/cm.

The results are given in Figs. 15 and 16. We see that the amplitude of HPM signal rises by factor of 3 in comparison to the data shown in Fig. 13. With aluminum strips, the main (filtered) components of the current during the emission are converging towards the frequency of 755 MHz. See Fig. 15, frame C.

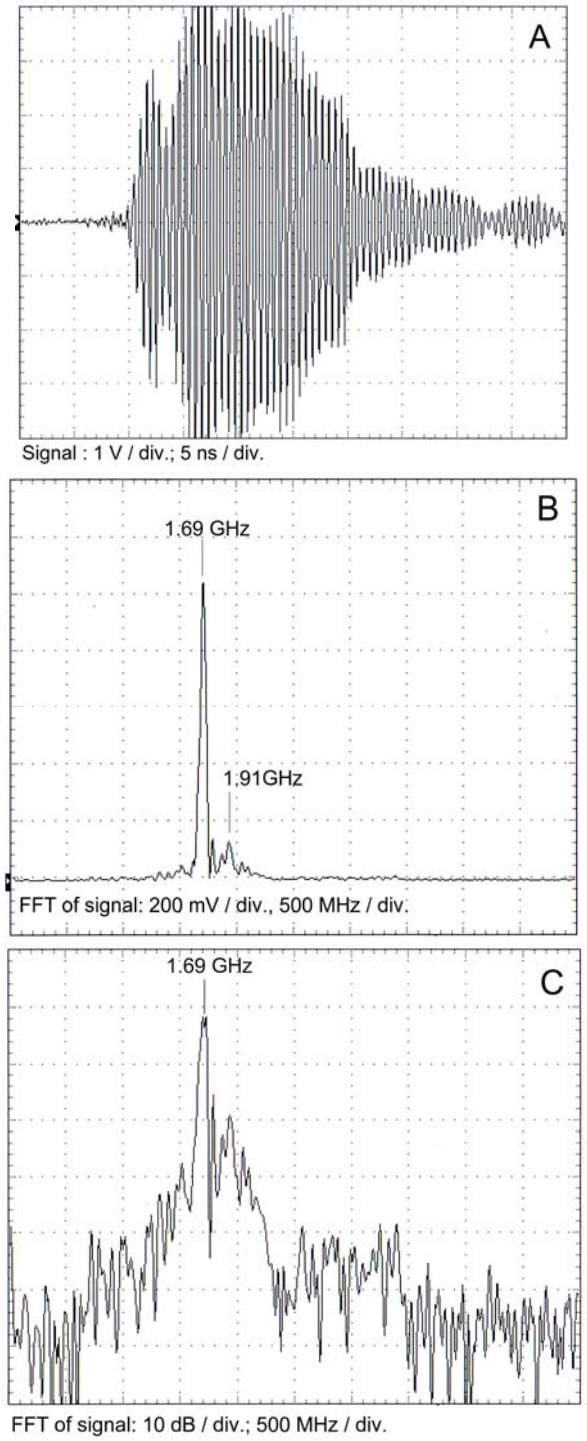

Figure 11; Frame A is the signal. **Frames B and C** are FFT of the signal. B-dot probe is used. 9-stage Marx generator charged to 18 kV / stage is applied and the energy stored in the generator is 22 J. B-dot probe is calibrated in the TEM-cell. For frequency of 1.69 GHz, the amplitude of the signal of 1 Volt corresponds to the electric field of 1.89 kV/cm.

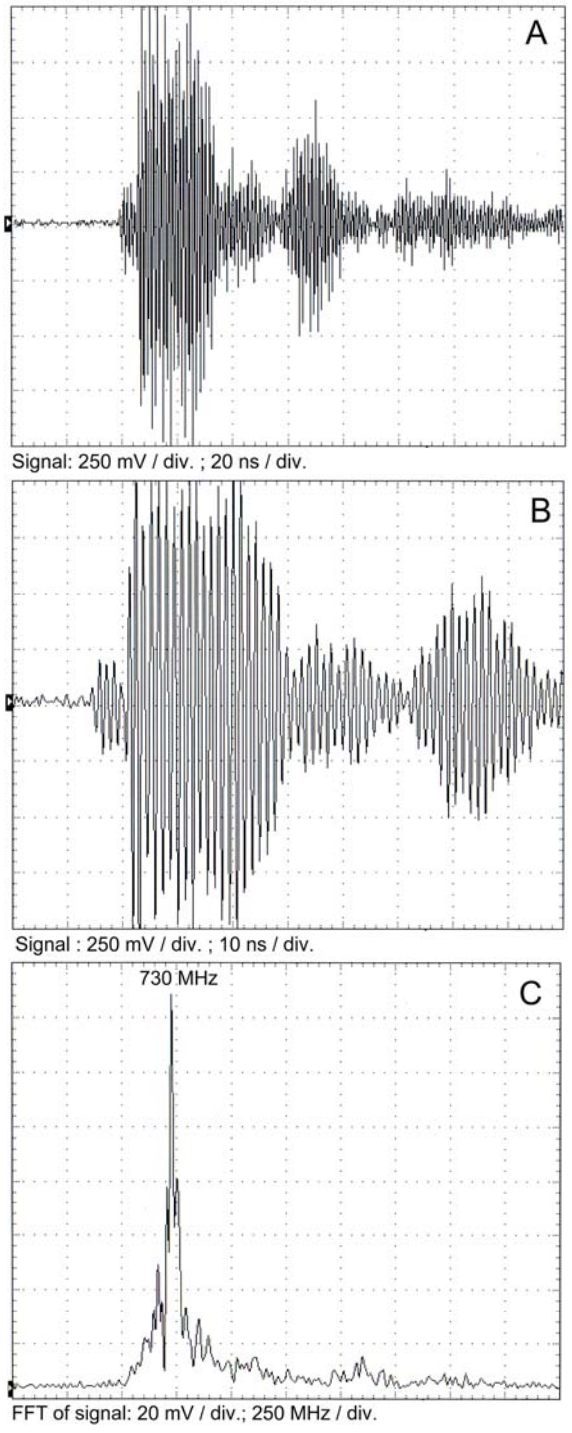

Figure 12; Frame A: Signal is recorded at the time scale of 20 ns per division. Frame B is the same signal presented on the time scale of 10 ns per division. Frame C is the FFT of signal. B-dot probe is used. 6-stage Marx generator is charged to 25 kV per stage and the energy stored in the generator is 84J.

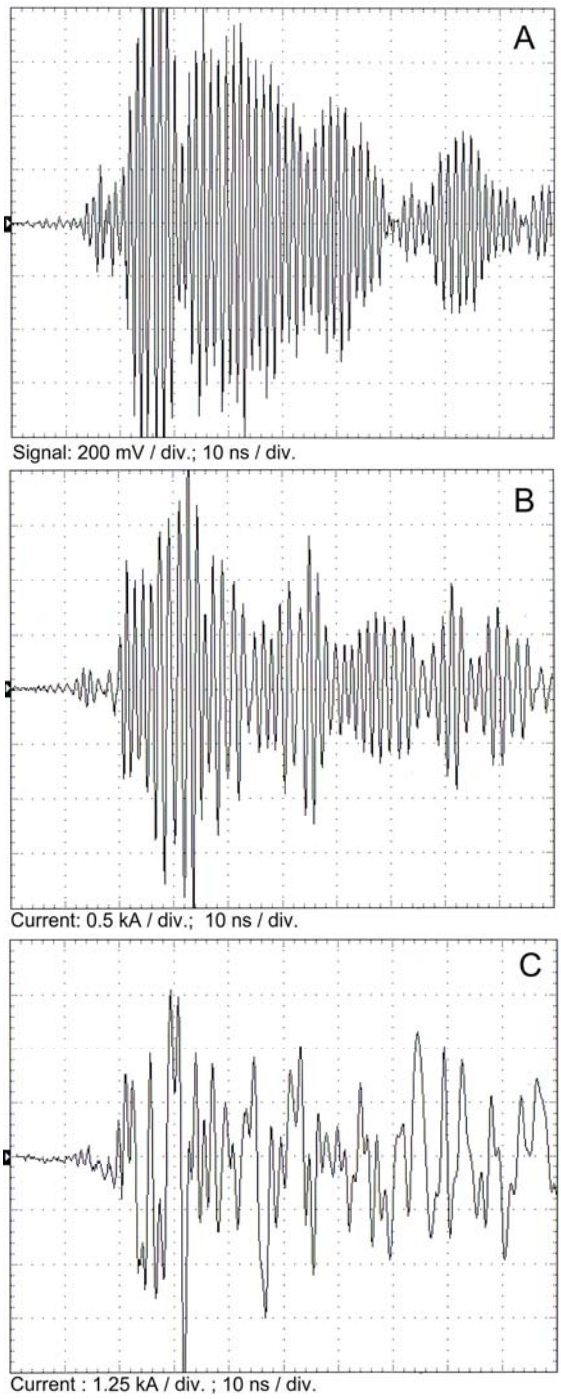

Figure 13. Frame A is signal. **Frame B** is the current recorded with high (500 MHz) pass filter. **Frame C** is the total current (The filter is not used). B-dot probe is used. 6-stage Marx generator is charged to 25 kV per stage and the energy stored in the generator is 84 J.

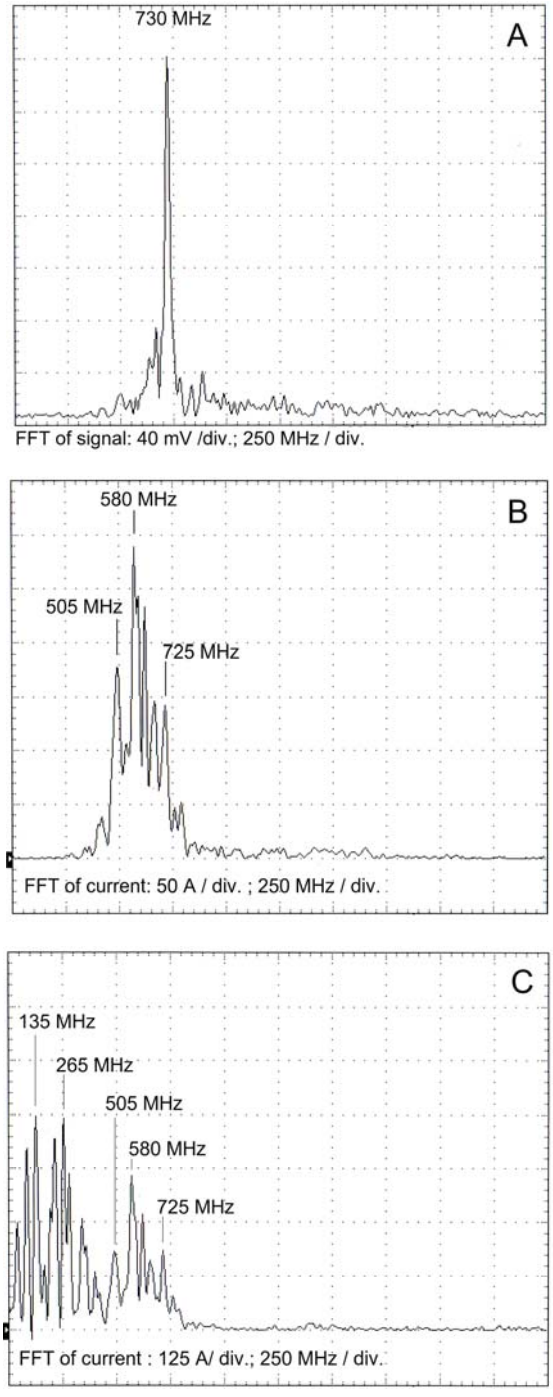

Figure 14. FFT of the data shown in Fig.13. B-dot probe is calibrated in the TEM-cell. For frequency of 730 MHz, the amplitude of the signal of 1 Volt corresponds to the electric field of 4.36 kV/cm.

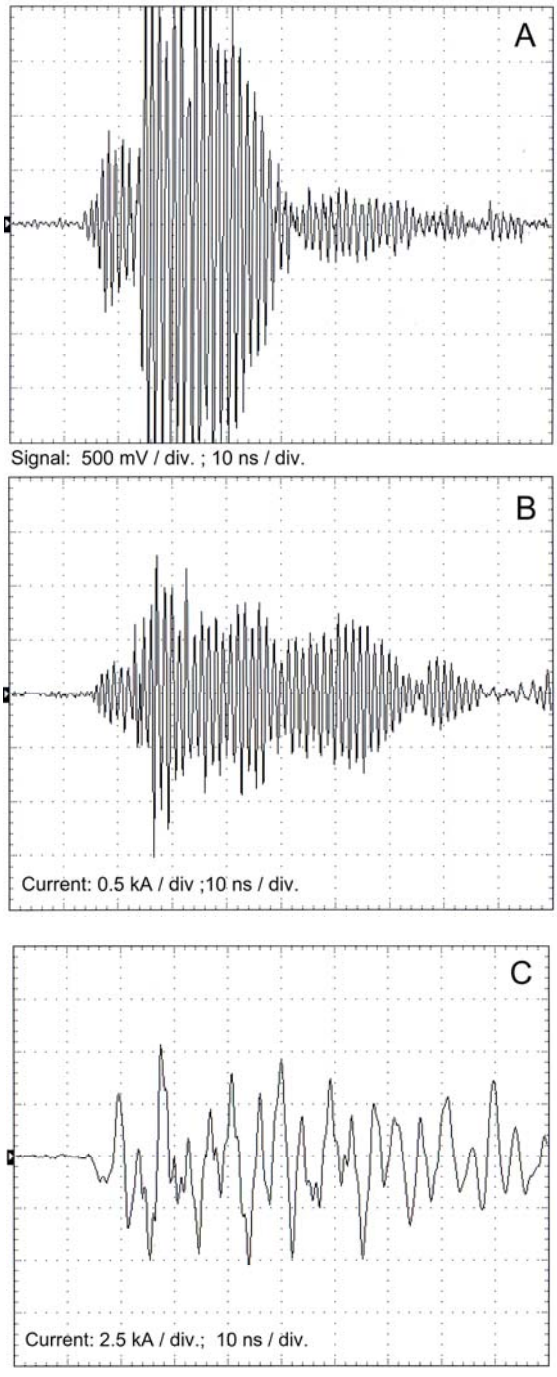

Figure 15. Frame A is signal. **Frame B** is the current recorded with high (500 MHz) pass filter. **Frame C** is the total current (The filter is not used). B-dot probe is used. 6-stage Marx generator is charged to 25 kV per stage and the energy stored in the generator is 84 J.

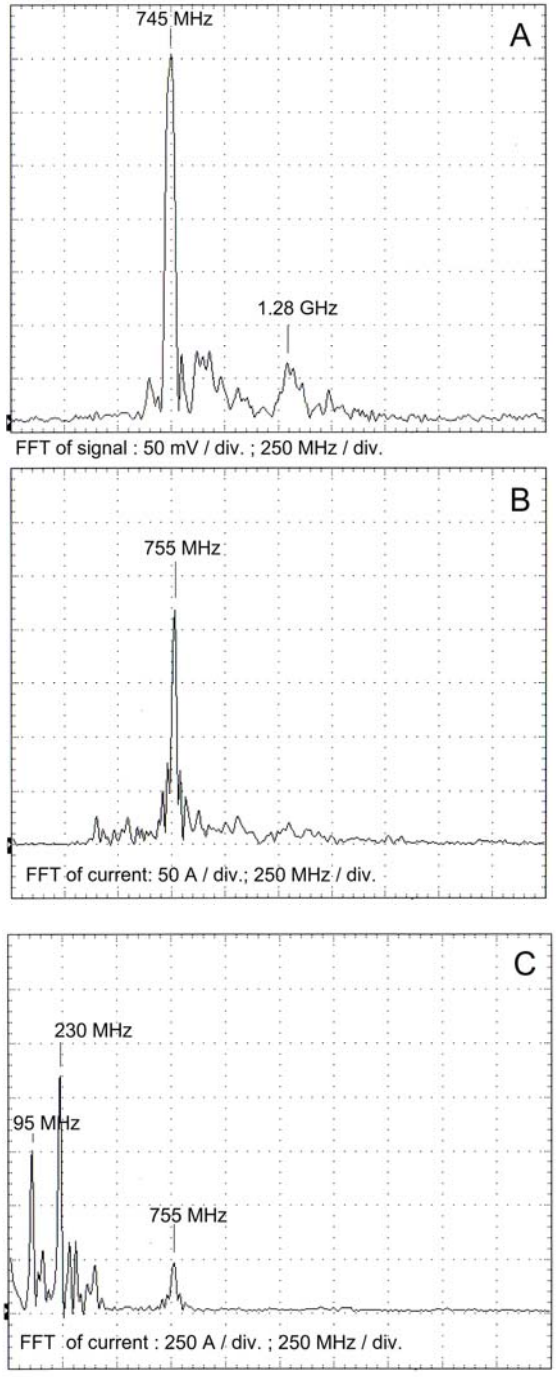

Figure 16. FFT of the data shown in Fig. 17. B-dot probe is calibrated in the TEM-cell. For frequency of 745 MHz, the amplitude of the signal of 1 Volt corresponds to the electric field of 4.28 kV/cm.

In comparison to Fig. 13, the condition for Fig. 15 has been changed in the following two ways. The length of the cylinder 6 of Fig. 7 has been extended by 50 % and the partial reflector, 8 was moved close to the helix about 10 cm. The idea is to contain more radiation flowing though the cylinder and to increase the amount of radiation reflected by the partial reflector. As expected, the signal in Fig. 15, frame A rises in comparison to that of Fig. 13, frame A. However, the surprise is that the frequency of the filtered current shown in Fig. 16, frame B is of higher value in comparison to that of the radiation.

As an additional proof that the glow plasma is responsible for the amplification of RF/HPM signal, a 59 cm long section from 10.6 μ CO_2 laser with 14 UV pre-ionization sources (placed along the longitudinal dimension, 7 UV sources on each side) is used. This section is the common sub-system of the CO_2 lasers that are made by Lumonics Ltd. The section is employed in the arrangement similar to the one given in Fig. 7. The array of 9 spark sources shown in Fig. 7 is removed. One electrode of the section is connected to the point A and the other electrode to the ground. The length of the cylinder, 6 is extended to cover the whole laser section. The helical antenna is attached to the other end of the section. After tuning the cavity to f=720 MHz, the trace similar to the one given in Fig. 12, Frame A is obtained

Discussion and conclusions:

The helix shown in Fig. 7 makes possible that the RF/HPM have many passes through the gain medium. The partially transparent reflector, 8 is set to reflect a small amount of radiation. We named these conditions: “weak coupling”. After tuning the system, reproducible self-similar data are obtained and some are shown in: Figs 8 to 16. The best gain was achieved at one of the following frequencies: 730-765 MHz, 1.21 GHz, 1.69 GHz and 1.96 GHz.

If the length of the cylinder is longer than the length of the helical line, the set-up of Fig. 7 cannot emit the frequency below f_c. Putting the partially transparent reflector in close vicinity at the end of the cylinder to reflect more radiation, we have the case of “strong coupling”.

During the process of tuning the cavity of the system with strong coupling arrangement, it was observed that the HPM at the output may rise 10 to 50 times and the power density (or power) up to 10^3 times in comparison to the case with the weak coupling. These results are presented in the Appendix of the brochure: “6-stage EMP/HPM Marx Generator” on the company’ website. There, it is shown that when 6-stage Marx generator is charged to 25 kV per stage, the maximum electrical field recorded inside the resonant cavity exceeds 580 kV/cm at frequency of 1.69 GHz. These data were recorded periodically in a run of 10 to 20 shots.

It was also found possible to tune 9-stage Marx generator to radiate in the mode of strong coupling and produce the ultra high field in the resonant cavity in the compact system. These data are shown in Figs. 8 to 10 of the brochure entitled: “HPM MCG simulator using 9-stage Rim Fire Marx Generator” and given on the company’ website.

In this brochure, Fig. 8 gives the “good results” obtained with week coupling. Figs 9 and 10 are the data with strong coupling, in which the ultra high fields are obtained. The partially transparent reflector is placed at the distance where N of Eq. 2 is 2. The brass electrode of 5 cm in diameter and 6 cm in height is used. The diameter of the outer cylinder is 4.5” (=11.43 cm).

In the recent experiments variations from shot to shot are reduced and the ultra high field are observed easily in the resonant cavity with strong coupling.

The main feature of the pulse of the HPM power observed so far at 1.96 GHz with “strong coupling”, is that the width of the pulse (FWHM), Δt is small and:

$$\Delta t * f = n, \qquad \text{where } n < 14 \qquad (4)$$

where, f is the frequency of the radiation and n the number of oscillations in the pulse. In these experiments, the structure energized by the 6-stage Marx generator (with 25 kV / stage) is tuned to radiate at 1.96 MHz. The electric field probe is used. The peak value of the electric field exceeds 300 kV/cm. The shape of the HPM power pulse and the width of the pulse (FWHM), Δt are obtained by multiplying the electric field by itself. For 20 shots fired, the averaged value of $\Delta t * f$ evaluated from Eq. 4 is 10.69 (equals to about 11 oscillations).

It could be of interest to note that from the data presented in the studies on superradiative microwave generation in X band and Ka band relativistic BWO’s [7], it appears that Eq. 4 holds even in their case. For example, we read from their Fig. 6 that, the super-radiance was recorded for $\lambda = 8$ mm (f=37.5 GHz) and the pulse width, Δt measured was 0.25 ns, making $\Delta t * f$ to be 37.5 GHz times 0.25 ns =9.375.

The gain at microwave frequencies does not necessarily imply “population inversion” such as that occurring in most lasers. There would have to be some type of gain medium (molecular, atomic, electronic) in which a population inversion could occur. In addition, the effect would have to be broadband since it appears that the “gain” can lead to microwave generation at different frequencies with the output frequency determined only by the dimensions of the resonator. Hence some other process is responsible for the build up of microwave energy in the resonator.

The idea is here put forward to state that the origin of the RF/HPM generation is due to the interaction of electromagnetic wave with runaway electrons of the corona (glow) plasma, i.e., the electromagnetic (radiation) wave of frequency, ω causes the space charge waves in the glow plasma.

Liu and Tripathi [8] have presented the case where the electrons are uniformly distributed along the x-axis and where the x-component of the electron velocity is $\Delta = v_x - \omega/k$ (when viewed in the frame moving with the phase velocity of the wave, ω/k). Here, k is the wave number. Liu and Tripathi divide electrons into two groups (A) $\Delta > 0$ and (B) $\Delta < 0$. Group A electrons (with the velocity, $v_x > \omega/k$) are accelerated in the accelerating zones of

the space charge waves and retarded in the decelerating zones to spend more time there. There is bunching of A group electrons in the retarding zones and the transfer of the energy from the high-speed electrons in the glow discharge into the incoming wave. The slower moving electrons ($v_x < \omega/k$) of group B tend to bunch in the accelerating zones, gaining the energy from the wave. The relative population of electrons with ($v_x > \omega/k$) and ($v_x < \omega/k$), determines the slope of particle velocity distribution function at $v_x = \omega/k$ and will decide the net damping (absorption of the wave/heating of plasma) or growth (amplification) of the electromagnetic (radiation) wave.

The second idea is here put forward to state that the origin of the RF/HPM generation is due to the presence of the runaway electrons in the corona discharge. Mesyats and Yaladin [9] have pointed out the macroscopic electric field at the micro-protrusions can reach the value of 10^6 to 10^8 V/cm for fast rising pulses. The runaway electrons in the cathode region acquire the energies from several tens to hundreds of kilo-electron volts in the cathode region. This region is several millimetres in width in atmospheric air. Some distance away from the accelerated region, the behaviour of the runaway electrons is similar to the behaviour of an electron beams from an external source. At micro-protrusion, the current density is in the range of 10^9 A/cm^2 and the mean velocity of runaway electrons was determined to be in the order of 10^{10} cm/sec.

Mesyats and Yaladin give the width (FWHM) of the runaway electron pulse to be 45 to 60 ps from the stationary protrusion or protrusions for a fast rising pulse. Fig. 2 indicates that energy supplied by the generator will bounce back and forth along the helical line and /or the brass electrode. Hence, it may be reasonable to assume that, the runaway electrons will appear continuously along the helical line and/or brass electrode.

The energy spectra curves of the runaway electrons have been measured by Tarasenko *et al* [10] and found to be in the range of 50 to 400 keV. Their graphs show that the runaway electrons are having several distinctive peaks at different energy levels. It will be of interest to find out whether tuning of the resonant cavity means searching for one of these peaks to get the maximum HPM from the system.

In general, propagation of an electromagnetic wave through the plasma is possible when the electron density is low enough so that the plasma frequency does not exceed the frequency of the electromagnetic wave. On the other hand, the experimental evidence presented, indicates that the amplitude of the electromagnetic wave is enhanced if the more intense corona plasmas are produced. The question now arises what value of electron density of runaway electrons is required to get a reliable production of powerful HPM data before the electron density of glow plasma makes impossible for the electromagnetic wave to penetrate the plasma. Further work is required to get full understanding of the response of the runaway electrons in corona plasma to the electromagnetic (radiation) wave. The idea is to find out whether the mechanism herewith proposed can be related with certainty to the phenomena known as the super-radiance (self-bunching and coherence).

References

[1] Benford J, Swegle J.A. and Schamiloglu E, *High Power Microwaves*, Second editions, (NY; Taylor & Francis Group), 2007

[2] Sarjeant W, Alcock, J and Leopold K., *Parametric study of a constant E/N pumped high-power KrF* laser*, IEEE Journal of Quantum Electronics, **QE-14**, No 3, March 1978, pp 177-184

[3] Kraus J. D and Marhefka, R. J *Antenna for all applications*, Third Edition, 2002 McGraw Hill-Boston

[4] See for example: http://en.wikipedia.org/wiki/Coherence_(physics)

[5] Baum C. E, Baker W. L., Prather W. D, Lehr J. M, O'Loughlin L. P, Giri D. V, Smith I. D, Altes R, Fockler J, McLemore D, Abdalla M. D and Skipper C, *"JOLT: A highly directed, very intensive impulse like radar,"* Proceedings of IEEE, **92**, 2004, pp 1096.

[6] Kekez M. M, *Understanding the HPM generation in atmospheric air with reference to small-size MCG*, IEEE Conference on Pulsed Power Conference, Washington, USA, June 28-July 2, 2009, pp 1139-1146

[7] Eltchaninov A.A, Korovin S. D, Mesyats, G. A, G. A, Pegal I.V, Rostov V. V, Shpak V. G., and Yalandin M. I, *"Review of studies of superradiative microwave generation in X band and Ka relativistic BWOs (review)"*, IEEE Transaction on Plasma science, **32**, 2004 pp 1093- 1099

[8] Liu S. C and Tripathi V. K, *"Interaction of electromagnetic waves with electron beams and plasmas"* 1994, (Salem-World Scientific Publication Co. Pte. Ltd.)

[9] Mesyats G. A and Yaladin M. I. *"On the nature of picosecond runaway electron beams in air"* IEEE Transaction on Plasma science, **37**, 2009 pp 785- 789

[10] Tarasenko V. F, Baksht E.H, Burachenko A. G, Kostyrya I. D, Lomaev M. I and Rybka D. V, *" Super-short avalanche electron beams in air and other gasses at high pressure"* IEEE Transaction on Plasma science (to be published)